JOURNAL OF AGRICULTURAL AND FOOD CHEMISTRY

Structural Characteristics of Phosphoramide Derivatives as Urease Inhibitors. Requirements for Activity

María Font,*,† María-José Domínguez,‡ Carmen Sanmartín,‡ Juan A. Palop,‡ Sara San-Francisco,§ Oscar Urrutia,§ Fabrice Houdusse,§ and José M. García-Mina§

Molecular Modeling Section and Synthesis Section, Department of Organic and Pharmaceutical Chemistry, University of Navarra, Irunlarrea 1, E-31008 Pamplona, Spain; and R&D Department, AFI-Roullier Group, Timac Agro España, Polígono Arazuri-Orcoyen, E-31160 Orcoyen, Spain

Taking as a reference the structural characteristics of a set of compounds that act as jack bean (*Canavalia ensiformis*) urease inhibitors, namely, phenylphosphorodiamidate (PPD), *N-n*-butylthiophosphorictriamide (NBPT), and *N-n*-butylphosphorictriamide (NBPTO), we have studied the structure−activity relationships of a series of phosphoramide derivatives for which the activity as urease inhibitors in both in vitro and in vivo assays is known. Molecular modeling studies were carried out, and the results highlighted the relevance of characteristics such as the presence of intramolecular hydrogen bonds, the volume of the fragment involved in the enzyme interaction, and the degree of conformational freedom as well as the HOMO orbital and atomic orbital contributions to the HOMO orbital, electron density, and PEM distributions on the activity of these compounds as urease inhibitors. These data, along with the preliminary docking study carried out, allow us to propose a union mode to the active site of the enzyme for these compounds.

KEYWORDS: Urease inhibitors; phosphoramides; fertilizers; urea

INTRODUCTION

Urease catalyzes the hydrolysis of urea in the final step of organic nitrogen mineralization to produce ammonia and carbamate. The carbamate produced during this reaction spontaneously decomposes to give a second molecule of ammonia and bicarbonate. Under ideal conditions, the ammonia is converted to ammonium, ready for plant uptake (*1*). However, under less than ideal conditions (soil pH <6−6.5) the ammonia can be lost to the atmosphere. Hydrolysis, the fundamental property of urea that greatly affects the management of urea as fertilizer, causes an abrupt overall pH increase, and this is the major cause of the negative side effects. The release of large amounts of ammonia into the atmosphere, as well as the plant damage induced by ammonia toxicity and the increase in soil pH, leads to significant environmental and economic problems (*2*).

The rapidly increasing importance of urea fertilizer in world agriculture (urea contains high nitrogen percentage, 46%) has stimulated research to find methods of reducing the problems associated with the use of this fertilizer. In this respect, increasing attention has been focused on the search for compounds that will inhibit urease activity, which is more intense on plant surfaces and organic residues than in soils, and thereby retard urea hydrolysis when applied to soils in conjunction with urea fertilizer. The development of urease inhibitors would lead to a reduction in environmental pollution and to an enhancement in the efficiency of nitrogen uptake by plants (*3*).

Urease represents a milestone in biological inorganic chemistry because it was the first enzyme to be crystallized (1926) and the first metalloenzyme to be characterized as a nickel-containing enzyme (1975) (*4*). The role of the active site metal ions, a bimetallic nickel center, and amino acid residues has been extensively studied but has not been totally elucidated to date.

Knowledge of the urease active site has been mainly provided by the crystal structures resolved for ureases from two bacteria, *Klebsiella aerogenes* (*5*) and *Bacillus pasteurii* (*6, 7*). The active site is located in the α subunits in all known ureases (*8, 9*). In the center, the nickel(II) ions (Ni1 and Ni2) are bridged by a carbamylated lysine through its oxygen (O) atoms, with Ni1 further coordinated by two histidines through their nitrogen (N) atoms, and Ni2 by two histidines through N atoms as well as by aspartic acid through its O atom. Furthermore, in the native enzyme the Ni ions are bridged by a hydroxide ion, which along with two terminal water molecules (one on Ni1 and the other on Ni2) and a third water molecule located toward the opening

* Author to whom correspondence should be addressed (telephone +34 948 425 600; fax +34 948 425 649; e-mail mfont@unav.es).
† Molecular Modeling Section, University of Navarra.
‡ Synthesis Section, University of Navarra.
§ AFI-Roullier Group, Timac Agro España.

10.1021/jf801786d CCC: $40.75
Published on Web 08/27/2008

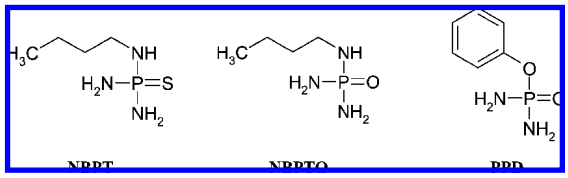

Figure 1. Structures of the urease inhibitors taken as references for the study carried out for the compounds.

of the active site, completes a tetrahedral cluster of solvent molecules that fill the active site cavity. It is this cluster that urea replaces when binding to the active site for the reaction. The fact that the crystallized ureases have an almost superimposable active site implies that this unit is common to all ureases, including jack bean urease (JBU), the crystal structure of which has not been resolved to date. The sequence of JBU (*10*) is closely related to the sequence of all bacterial ureases, suggesting a common evolutionary origin (*11*).

N-(*n*-Butyl)thiophosphorictriamide (NBPT, **Figure 1**) is the most effective compound currently available to retard the hydrolysis of urea fertilizer in soil and to decrease ammonia volatilization and nitrite accumulation in soils treated with urea. NBPT is a poor inhibitor of plant or microbial urease, but decomposes quite rapidly in soil to form *N*-(*n*-butyl)phosphorictriamide (NBPTO, **Figure 1**), which is a potent inhibitor of urease activity (*12*−*15*). Another phosphoric amide derivative, phenylphosphorodiamidate (PPD, **Figure 1**), was also found to inhibit urease (*16*), albeit in an indirect way.

The NBPTO molecule coordinates the two Ni atoms with a bidentate geometry. The oxygen atom and one amide group of the inhibitor molecule are engaged in the formation of a bridge between the Ni1 and Ni2 ions. Furthermore, another amide group of the NBPTO molecule forms a hydrogen bond with one oxygen atom of the carbamate bridge. The stability of the bidentate complex is strengthened by the formation of the hydrogen bond; as a result, the inhibitor molecule hooks the active site at three points: the two Ni atoms and one oxygen atom in the bridging carbamate group. This three-point interaction could explain the known ability of the NBPT molecule to act as a strong urease inhibitor (*17*). In this system the lateral alkyl chain can point toward the cavity opening.

In the case of PPD, it is observed that the actual inhibitor that binds to the enzyme active site is diamidophosphate (DAP), the product of the enzymatic hydrolysis of PPD (*18*). In the DAP-inhibited *B. pasterurii* urease (BPU) structure (*18, 19*), the tetrahedral DAP molecule almost perfectly replaces the cluster of water molecules seen in the native enzyme. In this way DAP is bound to Ni1 and Ni2 through one oxygen and one nitrogen atom, respectively; the second DAP oxygen atom, which is negatively charged, symmetrically bridges the two nickel ions, whereas the second nitrogen atom points away toward the cavity opening. Thus, the DAP binding does not alter the coordination and overall geometry of the active site. The probability of urea reaching the Ni ions is greatly reduced when the active site is locked by the inhibitor molecule.

Recently, we published the synthesis and urease inhibitor activity for a series of phosphoramide derivatives and also described the preliminary structure−activity relationships (*20*). The syntheses have been carried out by our team (*20*), according to methods reported previously. The overall structural variations carried out in the synthesis process, taking PPD as template, are shown in **Figure 2a**.

The urease inhibitory activity was determined in vitro by measurement of ammonium ions liberated (ionic HPLC) by urea hydrolysis (by urease enzyme action) for a fixed time, and the

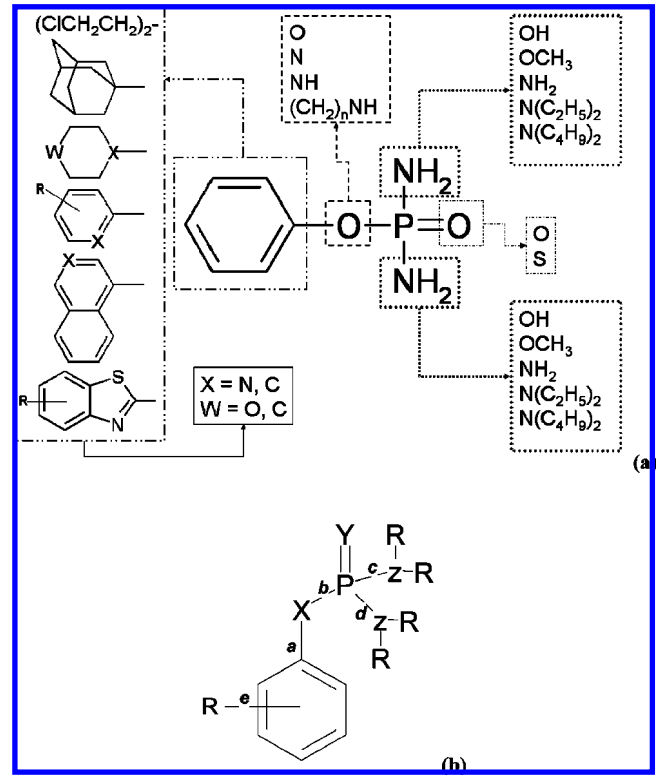

Figure 2. (**a**) Overview of structural variations carried out (*20*) for the described urease inhibitors, taking PPD (compound reference **1b**) as a template. (**b**) General structure for the analyzed compounds showing the bonds (*a*−*e*) selected for the conformational analysis.

results are expressed as inhibitory concentration 50 (IC_{50}, **Table 1**) of the phosphorated derivatives. The most active compounds (**6f**, **6k**, and **6p**) were also tested in in vivo (soils) assays. The activities in soils with different pH values were determined versus a control and using NBPT as a reference. The behaviors of compounds **6f** and **6p** were comparable to that of NBPT in neutral soils and in alkaline soils, with these compounds showing higher values than the reference compound, especially after 30 days of incubation (*20*).

In the analyzed structures (see **Figure 2b** for a general structure) the P═Y moiety (Y = O, S) adopts the function of DAP's P−O− moiety, whereas the surrounding nitrogen and/or oxygen atoms (X = O, NH; Z = O, N) can bind to Ni1 and/or Ni2 in a similar way to that observed for DAP. The lateral chain can be placed in the cavity opening in a similar way to that proposed for NBPTO. The introduction of alkylic chains on the terminal nitrogens and/or oxygens was proposed to modify the connection pattern of these atoms with the Ni ions as well as with the residues involved in the active site.

In the work described here we carried out a molecular modeling study on the aforementioned derivatives with the aim of evaluating the structure−activity relationships to gain an understanding of the activity shown by such compounds, to propose its union mode to the urease active site, and to try to explain the differences in chemical stability detected for some of the assayed derivatives.

The calculations were performed on a *Silicon Graphics* Octane2 workstation provided with the software package InsightII 2000 (*21*), on a Dell Precision 380 workstation, provided with the software package Discovery Studio v1.7 (*22*), and on a Dell Latitude D250 (Windows XP, PC) provided with the software package HyperChem Professional (*23*). The conformational freedom of the target compounds encouraged us to

Table 1. Experimental Data for the Analyzed Compounds

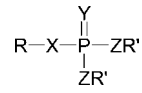

compd	R	X	Y	Z	R′	vol trajec[a]	vol L C[b]	E_{HOMO}[c]	E_{LUMO}[c]	ΔE_{L-H}[c]	Q_x[d]	Q_y[d]	Q_z[d]	IC_{50}[e] (μM)
1a	4-nitrophenyl	O	O	N	H_2	222.40	137.35	−9.974	−0.948	9.027	−0.708	−1.109	−0.980	0.063
1b[f]	phenyl	O	O	N	H_2	178.09	120.31	−9.179	0.414	9.593	−0.709	−1.113	−0.992	0.003
1c	3,5-dimethylphenyl	O	O	N	H_2	311.07	148.93	−9.044	0.461	9.504	−0.710	−1.113	−0.978	0.025
1d	4-benzyloxyphenyl	O	O	N	H_2	352.76	202.82	−8.664	0.337	9.001	−0.706	−1.114	−0.978	0.016
1e	4-methyl-2-nitrophenyl	O	O	N	H_2	204.26	152.17	−9.552	−0.840	8.712	−0.696	−1.119	−1.002	na[g]
2a	4-nitrophenyl	O	O	N	C_2H_5	nd[h]	nd	nd	nd	nd	nd	nd	nd	na
2b	4-nitrophenyl	O	O	N	C_4H_9	nd	nd	nd	nd	nd	nd	nd	nd	na
3	4-benzyloxyphenyl	O	S	N	H_2	465.40	216.30	−9.129	−0.607	8.522	−0.692	−1.275	−0.999	16.54
4	2-methylpyridyl	NH	O	O	H	184.57	122.74	−10.416	−0.612	9.804	−0.906	−0.559	−1.012	na
5a	3-methyl-2-pyridyl	NH	O	O	CH_3	nd	nd	nd	nd	nd	n.d	nd	nd	na
5b	2-benzothiazolyl	NH	O	O	CH_3	nd	nd	nd	nd	nd	nd	nd	nd	na
6a	bis(2-chloroethyl)	N	O	N	H_2	311.07	151.44	−10.203	1.038	11.241	−0.859	−1.143	−0.997	na
6b	1-adamantyl	NH	O	N	H_2	295.27	161.60	−10.111	1.808	11.918	−0.920	−1.146	−0.994	2.56
6c	1-naphthyl	NH	O	N	H_2	262.31	180.58	−8.870	−0.626	8.244	−0.883	−1.143	−0.996	0.53
6d	3-methoxyphenyl	NH	O	N	H_2	238.46	145.42	−9.366	−0.054	9.312	−0.888	−1.143	−0.995	5.57
6e	4-cyclohexylphenyl	NH	O	N	H_2	277.05	202.50	−9.402	0.046	9.448	−0.884	−1.144	−0.993	44.25
6f	4-methyl-2-nitrophenyl	NH	O	N	H_2	201.61	156.60	−10.053	−1.286	8.767	−0.853	−1.138	−1.003	0.003
6g	4-benzyloxyphenyl	NH	O	N	H_2	409.83	206.17	−9.187	0.041	9.228	−0.884	−1.145	−0.995	3.5
6h	2,5-dimethoxyphenyl	NH	O	N	H_2	289.82	165.81	−9.047	0.026	9.073	−0.867	−1.148	−0.993	na
6i	4-phenoxyphenyl	NH	O	N	H_2	346.38	192.05	−9.169	−0.217	8.952	−0.885	−1.143	−0.995	12.98
6j	2-(4-fluorophenyl)ethyl	NH	O	N	H_2	257.07	155.39	−9.553	−0.151	9.402	−0.926	−1.143	−0.995	0.048
6k	2-benzothiazolyl	NH	O	N	H_2	271.11	151.25	−9.049	−0.521	8.528	−0.798	−1.135	−0.995	0.002
6l	3-morpholinylpropyl	NH	O	N	H_2	298.19	171.83	−9.501	1.691	11.192	−0.926	−1.143	−0.994	0.71
6m	3-quinolyl	NH	O	N	H_2	264.11	157.03	−9.369	−0.763	8.606	−0.876	−1.138	−0.994	na
6n	phenyl	NH	O	N	H_2	195.37	123.61	−9.807	−0.018	9.825	−0.888	−1.144	−0.995	3.63
6o	4-nitrophenyl	NH	O	N	H_2	191.03	142.29	−9.550	−0.809	8.741	−0.843	−1.131	−0.998	0.30
6p	2-nitrophenyl	NH	O	N	H_2	242.46	140.51	−9.796	−1.024	8.773	−0.862	−1.137	−0.996	3.0
6q	2-phenylethyl	NH	O	N	H_2	242.27	152.33	−9.286	0.560	9.846	−0.932	−1.143	−0.996	0.014
6r	2-trifluoromethoxyphenyl	NH	O	N	H_2	254.50	154.95	−10.131	−0.635	9.496	−0.879	−1.141	−0.999	75
6s	2-ethoxycarbonyl-3-thienyl	NH	O	N	H_2	244.73	156.01	−8.769	−0.510	8.259	−0.8278	−1.135	−0.998	na
6t	6-ethoxy-2-benzothiazolyl	NH	O	N	H_2	307.37	188.70	−8.677	−0.448	8.229	−0.800	−1.136	−0.994	0.005
6u	6-fluoro-2-benzothiazolyl	NH	O	N	H_2	276.13	155.66	−9.076	−0.767	8.310	−0.796	−1.133	−0.994	0.005
6v	4-methoxy-2-benzothiazolyl	NH	O	N	H_2	322.76	174.31	−8.729	−0.506	8.222	−0.798	−1.136	−0.994	0.010
6w	4-methyl-2-benzothiazolyl	NH	O	N	H_2	206.06	167.24	−8.951	−0.504	8.447	−0.799	−1.135	−0.994	0.010
6x	3-nitro-2-pyridyl	NH	O	N	H_2	205.34	136.49	−10.033	−1.435	8.598	−0.778	−1.134	−0.990	0.070
6y	2-difluoromethoxyphenyl	NH	O	N	H_2	272.30	152.20	−9.839	−0.442	9.398	−0.870	−1.143	−0.995	20
6z	2-methoxy-4-nitrophenyl	NH	O	N	H_2	281.88	162.59	−9.642	−1.152	8.491	−0.822	−1.125	−0.996	0.020
7a	2-benzothiazolyl	NH	S	N	H_2	260.77	166.05	−9.214	−1.069	8.146	−0.814	−1.342	−1.009	2.96
7b	4-benzyloxyphenyl	NH	S	N	H_2	448.01	219.65	−9.143	−0.390	8.753	−0.902	−1.335	−1.011	na
7c	3-morpholinylpropyl	NH	S	N	H_2	323.38	185.41	−9.168	−0.067	9.100	−0.953	−1.336	−1.012	na
7d	4-phenoxyphenyl	NH	S	N	H_2	429.27	205.36	−9.201	−0.593	8.608	−0.902	−1.332	−1.002	na
7e	2-phenylethyl	NH	S	N	H_2	299.54	165.27	−9.164	−0.029	9.134	−0.954	−1.341	−1.012	13.86
7f	3-methylpyridyl	NH	S	N	H_2	253.99	146.23	−9.245	−0.212	9.033	−0.951	−1.350	−1.013	42.55
NBPTO	*n*-butyl	NH	O	N	H_2	207.58	119.96	−10.171	1.770	11.941	−0.932	−1.144	−0.996	nd
NBPT	*n*-butyl	NH	S	N	H_2	227.10	119.69	−9.177	0.029	9.206	−0.949	−1.332	−1.011	0.10

[a] Average volume for conformational trajectory, in Å^3. [b] Medium volume for representative lowest conformations (L C), in Å^3. [c] In eV. [d] Charge on atom. [e] See ref *20* for details. [f] PPD. [g] na, nonactive in biological assay. [h] nd, not determined.

use, as a template for building the initial conformation, the geometric data from the crystallographic structure for PPD (reference PPOSAM), obtained from the Cambridge Structural Database [CSD (*24*)]. The rotations selected for this analysis are summarized in **Figure 2b**.

In addition, the data collected on the chemical stability for some of the assayed derivatives in both the in vitro and in vivo tests allowed us to determine the bond order. According to the molecular orbital theory, the bond order (bo) is equivalent to the number of electrons in the antibonding molecular orbital minus the number of electrons in the bonding molecular orbital (MO) divided by 2. This parameter can be taken as a quantitative descriptor for the bond strength and is related to the aforementioned stability.

The X-ray structure of urease from diamidophosphate-inhibited *B. pasteurii* urease [2.0 Å resolution, 3ubp reference entry of the Brookhaven Protein Data Bank, PDB (*7, 25*)] was employed as a reference for the studies carried out with the aim of illustrating the possible union mode for our designed compounds.

MATERIALS AND METHODS

Molecular Modeling Methods. The initial computational work (conformational analysis, determination of volumes, orbitals, charge distribution, and determination of the pattern of intramolecular hydrogen bonds) was performed on a *SiliconGraphics* Octane2 workstation provided with the software package InsightII. The starting atomic coordinates were obtained from the structurally related Cambridge Structural Database structure PPOSAM (crystal model for PPD) [CSD System version 5.26: search and information retrieval with ConQuest (*26*) version 1.7; structure visualization with Mercury (*27*) version 1.3]. The three-dimensional models of the studied compounds were constructed, in the vacuum phase, using atoms and structural fragments from the *Builder* module (InsightII). The protocol can be summed up as follows: (a) initial construction of the model; (b) hierarchized

Table 2. Molecular Orbital Coefficients of HOMO of Representative Compounds

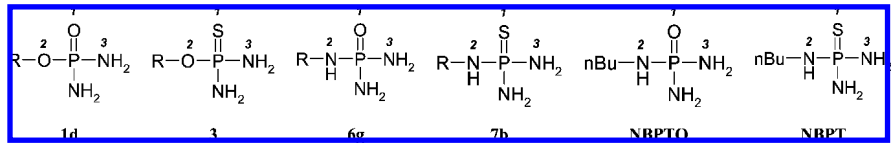

		AO coefficients (for HOMO)					
compd	AO	**1d**	**3**	**6g**	**7b**	NBPTO	NBPT
1	2s	−0.00037	0.04948	0.00563	0.00023	0.00340	−0.00147
	2px	−0.00252	0.10062	−0.05995	0.97254	0.22789	−0.91087
	2py	0.00136	−0.24081	−0.02534	0.10149	−0.08597	0.34171
	2pz	−0.00072	0.01786	0.05483	0.02344	−0.20528	−0.09308
2	2s	0.00283	−0.18113	0.03502	0.00132	−0.01128	−0.01778
	2px	−0.01506	−0.20702	−0.11209	−0.09701	−0.59179	0.07376
	2py	−0.00263	−0.11567	−0.04308	−0.01172	0.29163	−0.05806
	2pz	−0.00512	0.18734	0.02896	−0.00011	0.36279	0.04470
3	2s	0.00146	−0.00007	−0.00765	−0.05995	0.00625	−0.04539
	2px	−0.00289	−0.00078	−0.03119	0.01122	−0.02320	0.03169
	2py	0.00055	−0.07038	−0.00532	−0.08030	−0.05432	−0.05065
	2pz	−0.00321	0.02658	−0.00200	−0.02518	−0.07464	−0.07781

[a] R = 4-benzyloxyphenyl.

systematic conformational analysis [determination of the rotation-sensitive bonds; selection of a 30° window to check each selected dihedron; first filtration, elimination of the conformations that are indistinguishable by symmetry; second filtration, elimination of conformations that present steric impediments; third filtration, calculation of the energy of conformations and elimination of those conformations having a relative energy of >10 kcal/mol at a global minimum; fourth filtration, optimization of the geometry of the conformations and elimination of those having a relative energy of >10 kcal/mol at a global minimum; all molecular mechanics calculations carried out using the consistent valence electrostatic force field Extensible Systematic Force Field, ESFF (*28*) (*Search and Compare* module, InsightII]; (c) analysis of conformational trajectory (*Analysis* module InsightII) and selection of representative lowest energy conformation [root mean square (rms) deviations of the structures monitored]; (d) mechanoquantics optimization of the conformations obtained in the previous step with the molecular orbital calculations package *Mopac* [AM1 (*29*) and PM3 (*30*) semiempirical approaches, *AMPAC/MOPAC* built into the InsightII module].

The molecular electrostatic potential (MEP) values of some representative derivatives and reference compounds (NBPT, NBPTO, and PPD) were calculated on a Dell Precision 380 workstation, provided with the software package Discovery Studio (DS) 1.7., using the implemented Electrostatic Potential Protocol (EPP). This protocol calculates the electrostatic potential of a molecule by solving a nonlinear Poisson−Boltzmann equation using the finite difference method (*31*), as implemented in the DS Delphi V4 (*32, 33*) release 1.1 module. Once the molecule had been constructed, the optimization of the geometry of the initial conformations was carried out by applying the Dreiding minimizer [Dreiding forcefield (*34*); Steepest Descent algorithm with a criterion convergence of 10^{-6}]. The potential was calculated on grid points per side (65 × 65 × 65), and the percentage of box to be filled was set to 50%. The outer dielectric and the dielectric in the medium were set to 80.0 and 2.0, respectively. An ionic exclusion radius of 2.0 Å, a solvent radius of 1.4 Å, and a solvent ionic strength of 0.145 M were applied. CHARMM (*35, 36*) charges and radii were used for this calculation. Values of the electrostatic potential of <−250 were considered for the comparative analysis of the MEP distribution for the analyzed derivatives.

Bond Order. This work was performed on a Dell Latitude D250 (Windows XP, PC) provided with the software package HyperChem Professional. The lowest energy conformations of selected compounds, obtained after the conformational analyses carried out previously, were submitted to a new minimization (eigenvector following algorithm, with a criterion convergence $<10^{-3}$ kcal Å^{-1} mol^{-1}) with the PM3 semiempirical method. The bond order was directly computed for the selected compounds and evaluated as an approximate quantitative descriptor for the bond strength.

Active Site Model. The X-ray structure of urease from diamidophosphate-inhibited *B. pasteurii* urease 3ubp (*7*) was employed to build (*Builder* module InsightII) our active site mode. The key residues involved in the urea hydrolysis reaction and considered for our model are His137, His139, Ala170, KCX220 (carbamylated lysine), His249, His275, His280, His323, Asp363, Ala366, Met367, and the two nickel ions Ni1 and Ni2. To achieve an overall charge of zero on the active site, two histidines were taken as deprotonated. The neutral Nε1−H tautomeric form of the imidazolic ring was chosen for the remaining two histidines owing to its lower energy (*37*). According to this arrangement of the ligands, each nickel ion coordinates two imidazole rings. The enzyme crystallized in the presence of PPD [ref PDB: 3ubp] contains the tetrahedral transition-state analogue DAP bound to the two nickel ions. In the native urease [ref PDB: 2ubp (*6, 7*)] the ligands of the nickel atoms are four imidazoles (His249 and His275 interact with Ni1; His137 and His139 with Ni2), one carboxylate (Asp363 coordinating Ni2), and a water molecule that is coordinated by Ni2 and the bridging carbamylated lysine (KCX).

Proposal for the Union Mode. The first approach for the proposal of a union mode for representative compounds in the catalytic site in the enzyme was constructed by taking the complex DAP−BPU as a template (3ubp). The representative low-energy conformations obtained for selected compounds were superimposed through a manual docking process (*Biopolymer* module, InsightII), taking as a superposition pattern the P−O− moiety on the DAP for P═O, whereas group X was systematically superimposed onto the rest of the O and/or N atoms of this molecule in a search for the best orientation of the R group toward the open cavity of the active center.

RESULTS AND DISCUSSION

Once the models for the compounds had been constructed, the initial geometries were fully minimized to an energy gradient below 10^{-3} kcal mol^{-1} Å^{-1}. The minimum energy conformers were superimposed, with the P═Y moiety and the surrounding nitrogens or oxygens from the central structure taken as adjusting atoms. The effectiveness of the superimposed models was evaluated in terms of the rms values obtained. The energy differences between the different conformations analyzed for each trajectory were in the range of 2−5 kcal.

With respect to the structural variations that affect the fragment R, the more active compounds are those that incor-

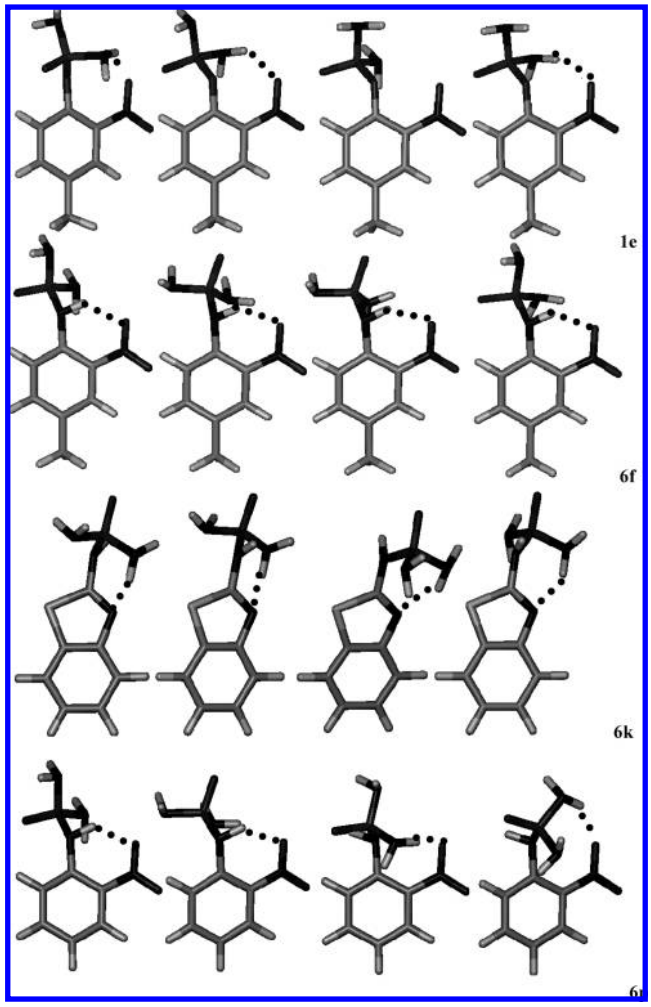

Figure 3. Intramolecular hydrogen bond pattern (dotted line) for (**a**) **1e**, (**b**) **6f**, (**c**) **6k** and (**d**) **6p** low-energy representative conformations.

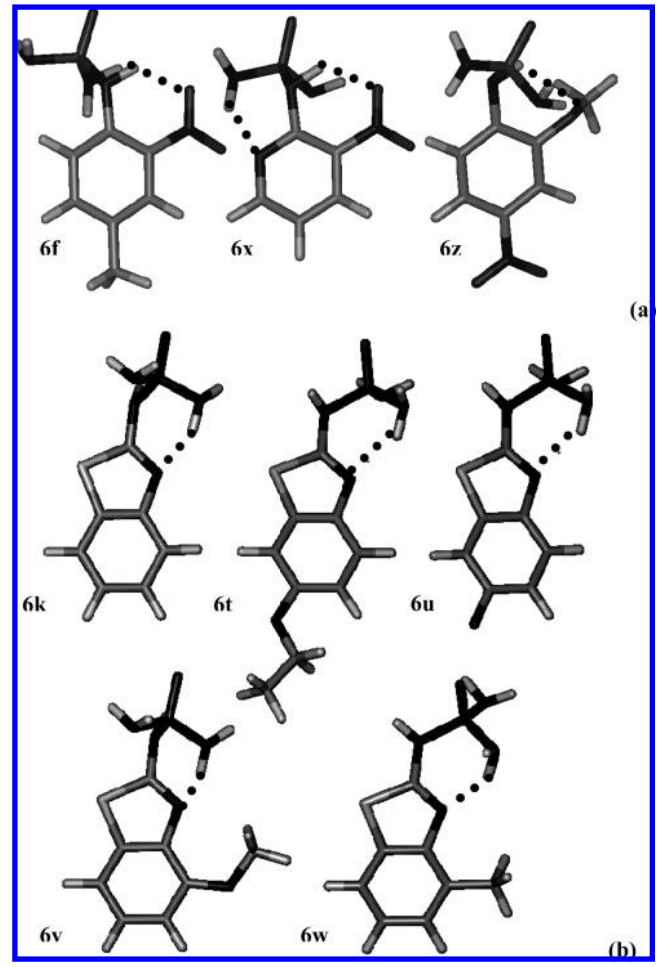

Figure 4. Examples of contributions of the intramolecular hydrogen bonds (dotted line) to the lowest energy conformation in (**a**) aryl and pyridyl derivatives (**b**) benzothiazolyl derivatives.

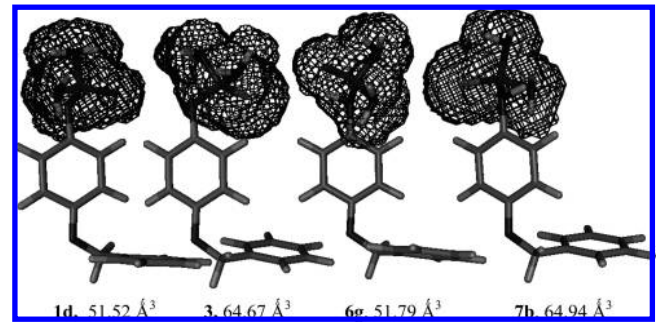

Figure 5. Comparison of the volumes (average value obtained from the lowest energy conformations) of the fragment—P(═Y)$(NH_2)_2$, in relation to Y (= O, S), shown on a representative low-energy conformation for the benzyloxy derivatives.

porate a flat aromatic or heteroaromatic ring, with great variability possible in terms of the volume of such a ring. In fact, the data obtained in the conformational analysis show that some level of biological activity is maintained in the compounds despite the wide range of overall volumes found (**Table 1**). Thus, for the most active compounds (with $IC_{50} \leq 0.07$ μM) the lowest conformational trajectory volume (178 Å^3) is obtained for compound **1b** (PPD), with a volume of 120.31 Å^3 for the lowest energy conformation, whereas the highest ones correspond to **1d** with values of 352.7 Å^3 and 202.8 Å^3 for the trajectory and the lowest energy conformation, respectively. This situation is compatible with our starting hypothesis that these fragments would arrange in a preferred conformation in which they were oriented toward the free cavity of the enzyme.

As far as the substituent present in the ring is concerned, it can be observed that the inhibitory activity is favored by the presence of groups such as NO_2 or OCH_3 located in position 2 of the aryl derivatives (for example, compound **6f** or **6z**), groups that are able to participate in intramolecular hydrogen bonds established between this group and fragment X, when X = NH, or fragments ZR′, when ZR′ = NH_2. The formation of these intramolecular bonds can facilitate the adoption of the most favorable conformation for the effective interaction with the active site of the enzyme. Representative low-energy conformations obtained for **1e** (X = O) and **6f** (X = NH), aryl compounds with the substituents NO_2 and CH_3 in the 2- and 4-positions, respectively, for **6k** (X = NH), a benzothiazole derivative, and for **6p** (X = NH), an aryl derivative with NO_2 in the 2-position, are shown in **Figure 3**. As can be observed, for the inactive compound **1e** the intramolecular hydrogen bonds are preferentially formed with the terminal NH_2 moiety, whereas in most of the lowest energy conformations for compound **6f** (IC_{50} = 0.003 μM) the bonds are preferentially formed with the X = NH moiety, thus potentially leaving the P═Y fragment accessible for the interaction with the active site. Finally, compound **6p** (IC_{50} = 3 μM) shows an intermediate bond pattern. In the case of compound **6k** (IC_{50} = 0.002 μM), although in the low-energy conformations the bond involves the terminal NH_2, it is observed that the fragment P═Y stays in the appropriate orientation. In this case, the nitrogen of the benzothiazole ring

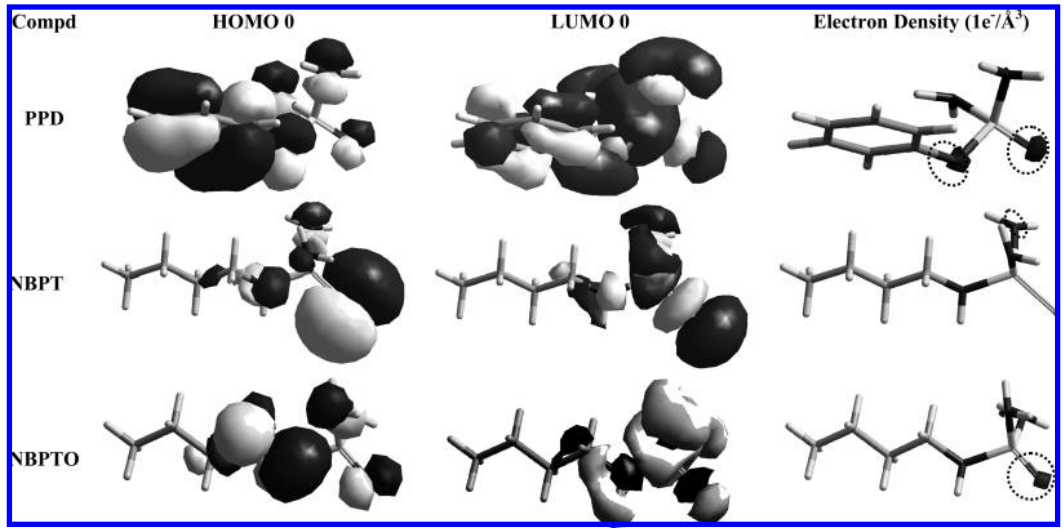

Figure 6. Influence of the X (O or NH) and Y (O or S) fragments on the HOMO 0, LUMO 0, and electronic density distribution (dotted line), for reference urease inhibitor compounds PPD (X = O, Y = O), NBPT (X = NH, Y = S), and NBPTO (X = NH, Y = O), shown on a low-energy conformation.

acts as a hydrogen bond acceptor. In addition, these substituents in the aryl moiety as well as the heteroatoms on the heteroaryl cycle can participate in intermolecular hydrogen bonds established with the surrounding residues near the Ni ions in the urease active site, thus reinforcing the union with the enzyme.

Several examples of the contribution of the intramolecular hydrogen bonds to the lowest energy conformation in aryl (**6f** and **6z**), pyridyl (**6x**) and benzothiazolyl (**6k**, **6t**, **6u**, **6v**, and **6w**) derivatives are shown in **Figure 4**. It can be seen that, for these heteroaryl derivatives, the heteroatoms located in the ring can act in a similar way to that proposed for the groups in the 2-position of the aryl derivatives.

The X fragment, which acts as a bridge between R and P, introduces greater conformational freedom and flexibility. As a result, it is observed that phenylphosphonic acid, which was synthesized and evaluated as a reference, was totally inactive in our tests. This observation can be explained by considering that the absence of the X group makes it impossible to adopt an appropriate conformation for an effective interaction with the active site. In addition, the absence of X also entails the loss of a center involved in the formation of hydrogen bonds.

With respect to the volume of the X—P(=Y)(ZR′)$_2$ moiety, the presence of alkylic chains on the Z heteroatoms (compounds **2** and **5**) leads to the disappearance of the inhibitory activity, and this could be related to a steric impediment. The heteroatom Y also influences the inhibitory activity, and this is related to the average volume value of this fragment. Thus, the volume of the X—P(=Y)(ZR′)$_2$ moiety in compounds where Y = S is slightly greater than the value calculated for the compounds in which Y = O. In addition, in this case the activity decrease could be associated with steric factors, among other possible causes that will be discussed below. As an example, the average values of the volume for the X—P(=Y)(NH$_2$)$_2$ moiety calculated on a representative low-energy conformation for the benzyloxy derivatives **1d** (X = O, Y = O), **3** (X = O; Y = S), **6g** (X = NH; Y = O), and **7b** (X = NH; Y= S) are given in **Figure 5**.

Our initial proposal stated that the compounds must interact with the Ni(II) ions and surrounding residues in the active site of the enzyme through the Y, X, and/or Z heteroatoms bonded to P. In accordance with this proposal, we selected the atomic charge, the location, and atomic orbital contribution to the HOMO 0 orbital, the electron density, and the MEP distribution as descriptor parameters for the first structure−activity relationships based on quantum chemistry semiempirical calculations. The data are collected in **Table 1**, and schematic views are provided in **Figures 6** and **7**.

With respect to the atomic charges located on the X—P(=Y)(ZR)$_2$ moiety (**Table 1**), it is possible to propose that the displacement of the negative charge toward Y and Z brings about a decrease in the target activity. Thus, it can be observed that, in general, the replacement of O by sulfur (S) in the fragment Y causes an increase in the negative charge on this atom and the adjacent N, a situation that is possibly related to the observed decrease in activity.

Generally, a direct relationship is not observed between the variation in the energy values for HOMO 0 and LUMO 0 orbitals for the structural modifications carried out and the activity of the compounds. Similarly, it is not possible to establish a relationship between the LUMO−HOMO gap energy values and the activity of the studied compounds (**Table 1**). Nevertheless, the lack of activity for derivatives in which Y = S can be ascribed, in addition to the steric factors mentioned above, to the distribution of the HOMO orbital, to the atomic orbital contribution to this orbital, and to the electron density located on Y. If one considers as a starting point the data concerning these parameters obtained for PPD, NBPTO, and NBPT (**Figure 6**), it can be deduced that the replacement of O by S results in a marked increase in the HOMO location over the S, whereas the deep negative zone that appears on O for the derivatives with P=O (for example, PPD or NBPTO) disappears for analogous compounds with P=S (for example, NBPT). In a similar way, the distribution and atomic contribution for the orbital HOMO 0 is observed. In the P=S derivatives the S atom contributes to a greater extent to this orbital, whereas for P=O derivatives the contribution is much smaller for the O. In the benzyloxy derivatives, which are taken as representative compounds for illustrative purposes (**Figure 7**), a similar type of behavior is observed. Compounds **1d** (X = O, Y = O, Z = NH$_2$, IC$_{50}$ = 0.016 μM) and **6g** (X = NH, Y = O, Z = NH$_2$, IC$_{50}$ = 3.5 μM) show HOMO and electronic density distribution similar to that found in PPD or NBPO. In compound **7b** (X = NH, Y = S, Z = NH$_2$, inactive) the HOMO 0 orbital is located on S and the electron density that is located on Y in the oxo derivatives disappears.

The coefficients for the development of the HOMO for the benzyloxy derivatives, the squares of which show the contribu-

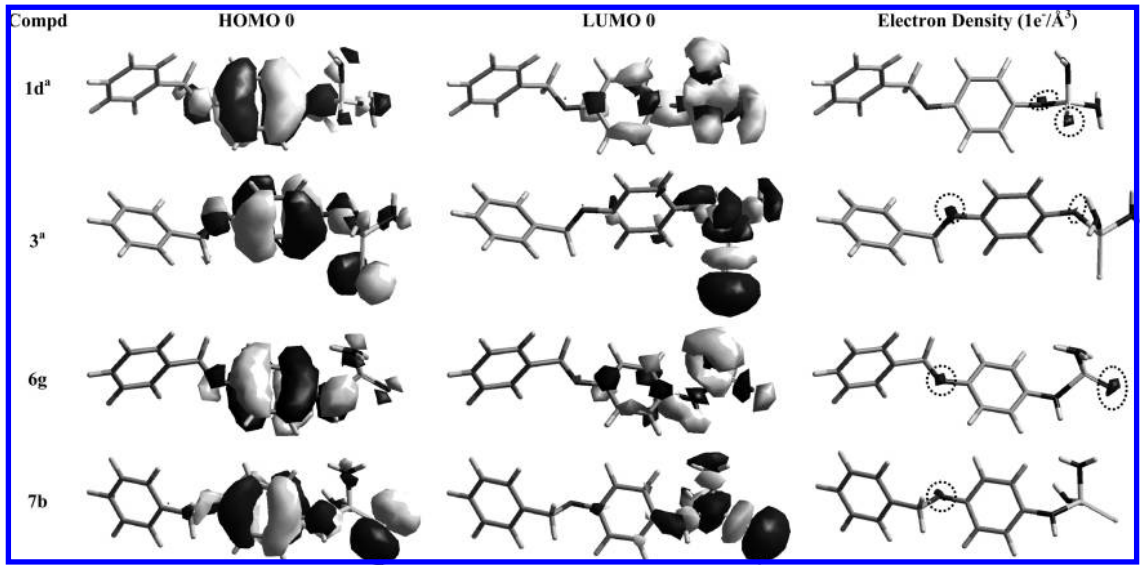

Figure 7. Influence of the X (O or NH) and Y (O or S) fragments on the HOMO 0, LUMO 0, and electronic density distribution (dotted line), for representative selected compounds (benzyloxy derivatives), shown on a representative low-energy conformation. [a]Data previously reported (*20*).

Table 3. Comparative MEP[a] Distribution (Lowest Energy Conformation) for Representative Compounds

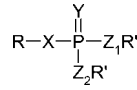

compd	R	X	Y	Z_1	Z_2	R′	IC_{50}[b](μM)	PEM_x	PEM_y	PEM_{z1}	PEM_{z2}
1d	4-benzyloxyphenyl	O	O	N	N	H_2	0.016	−473.0	−479.2	−318.5	−379.1
3	4-benzyloxyphenyl	O	S	N	N	H_2	16.54	−428.4	−278.8	−361.5	−443.3
6g	4-benzyloxyphenyl	NH	O	N	N	H_2	3.5	−199.4	−545.0	−393.4	−489.9
7b	4-benzyloxyphenyl	NH	S	N	N	H_2	na[c]	−177.9	−285.3	−250.5	−275.6
NBPTO	*n*-butyl	NH	O	N	N	H_2	nd[d]	−380.7	−698.4	−391.4	−733.9
NBPT	*n*-butyl	NH	O	N	N	H_2	0.10	−261.6	−330.7	−293.5	−449.3

[a] Kilocalories per mole. [b] See *20* for details. [c] na, nonactive in biological assay. [d] nd, not determined.

Table 4. Bond Order (bo) Values Calculated for Representative Compounds (Lowest Energy Conformation)

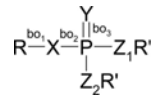

compd	R	X	Y	Z_1	Z_2	R′	bo_1	bo_2	bo_3
1b[a]	phenyl	O	O	N	N	H_2	1.039	0.557	1.314
6n	phenyl	NH	O	N	N	H_2	1.045	0.724	1.285
1d	4-benzyloxyphenyl	O	O	N	N	H_2	1.025	0.560	1.296
3	4-benzyloxyphenyl	O	S	N	N	H_2	1.019	0.634	1.126
6g	4-benzyloxyphenyl	NH	O	N	N	H_2	1.047	0.616	1.295
7b	4-benzyloxyphenyl	NH	S	N	N	H_2	1.027	0.774	1.114
1e	4-methyl-2-nitrophenyl	O	O	N	N	H_2	1.079	0.478	1.308
6f	4-methyl-2-nitrophenyl	NH	O	N	N	H_2	1.1511	0.638	1.291
6k	2-benzothiazolyl	NH	O	N	N	H_2	1.135	0.552	1.318
NBPTO	*n*-butyl	NH	O	N	N	H_2	0.984	0.726	1.270
NBPT	*n*-butyl	NH	O	N	N	H_2	0.978	0.814	1.103

[a] PPD.

tion of each atomic orbital to the electron density in a given MO (*38*), are listed in **Table 2** along with those for the reference compounds NBPTO and NBPT. Because the AM1 semiempirical method uses a valence basis set, only the atomic orbitals of the valence shell are considered in the development of the MO: 2s, 2px, 2py, and 2pz for N, O, and S and 1s for H. For the sake of brevity, only data that refer to target heteroatoms are presented. It can be observed that the replacement of O by S leads to a significant increase in the contribution of the 2px atomic orbital to the electronic charge density of the HOMO levels, a situation that is particularly marked for compound **7b**, for which the lack of activity could be associated with the dominant contribution of the S atom. In relation to the previous observations, and with respect to the values and distribution of the molecular electrostatic potential (MEP), the structural modifications that entail a deepening of the negative values on the $X-P(=Y)(ZR)_2$ moiety generally seem to cause a decrease in the activity (**Table 3**).

On the other hand, several of the studied compounds showed a certain level of chemical instability, especially the O-substituted diamidophosphate derivatives **1**. This instability was also detected, albeit to a lesser extent, for the benzothiazolyl

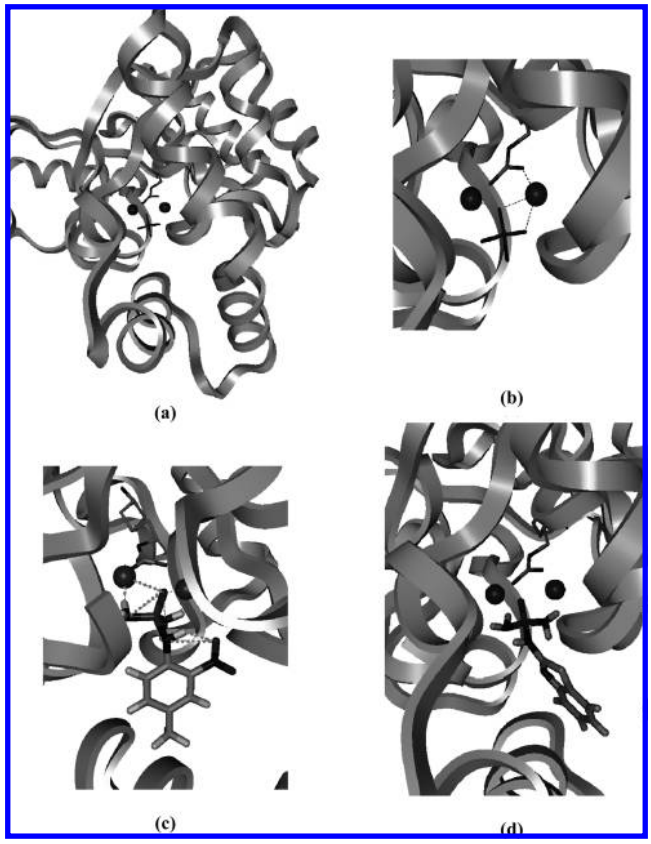

Figure 8. (**a**) Schematic representation of the urease active site (ref pdb: 3ubp). Catalytic residues are represented as ribbons, modified lysine and DAP as tubes, and Ni^{2+} atoms as spheres. (**b**) Detail of the binding mode for DAP. (**c**) Detail of the proposed binding mode for **6f** (tubes), showing the hydrogen bonds (dotted line) that contribute to the stabilization of the lowest energy conformation. (**d**) Detail of the proposed binding mode for **6k** lowest energy conformation (tubes). See Materials and Methods for details.

derivatives **6k**, **6t**, **6u**, **6v**, and **6w**. If one also considers the data cited previously concerning the inhibition mechanism of BPU by PPD, according to which PPD undergoes hydrolysis to give diaminophosphate (DAP) and phenol, it was decided to study the influence of the different structural modifications carried out on the bond order (bo) values calculated by means of the quantum AM1 semiempirical approach. The bo values were taken as a quantitative descriptor for the bond strength, and the values obtained were related to the aforementioned stability. The bo data for some of the compounds studied are given in **Table 4** and are grouped according to structural similarity. Thus, comparison of the data obtained for PPD (**1b**, X = O) and **6n** (X = NH) shows that the change from O to NH increases considerably the bo value in the X—P moiety, and these data could be related to the observed increase in stability for **6n**. This behavior is similar in all of the evaluated compounds. With respect to benzothiazolyl derivatives, it was found that the X—P bond has the lowest bo values (taking **6k** as an example), which would explain its lower relative stability.

A preliminary docking study was carried out for some of the compounds to evaluate the possible interaction between the enzyme active center and the active compounds, thus exploring the previously proposed characteristics related to their activity as urease inhibitors. A manual superposition of the selected lowest energy conformations (obtained from the conformational analysis described previously) was carried out by taking the DAP molecule in the complex DAP—BPU (ref PDB: 3ubp) as a superposition template (**Figure 8a**,**b**). The initial orientation and position of the ligand were made according to the superposition of the P═Y moiety on the P—O− fragment of DAP, whereas group X was systematically superimposed onto the rest of the O and/or N atoms of this molecule in a search for the best orientation of the R group toward the opened cavity of the active center and for the most favorable hydrogen bonding pattern.

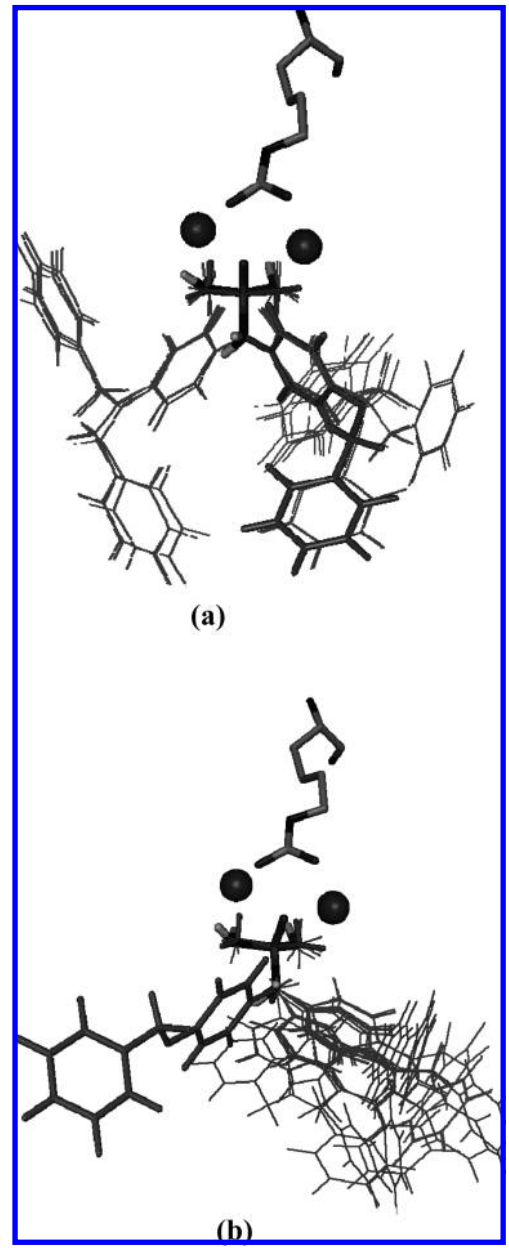

Figure 9. Simplified representation of the urease active site, showing the carbamoyl-modified lysine residue (tubes) and the Ni^{2+} ions (spheres) with superposition in the active site of the low-energy conformations for (**a**) **1d** and (**b**) **6 g**. Lowest energy conformations are represented as solid gray tubes. See Materials and Methods for details.

Schematic views of the results obtained for compounds **6f** and **6k** are shown in panels **c** and **d** of **Figure 8**, respectively. It can be observed that the P═O fragment is located between the Ni(II) ions, with the NH_2 and NH groups oriented toward the residues that surround the Ni ions, whereas the aryl group orients itself toward the open enzyme cavity. The manual docking carried out for the lowest energy conformation considered for **6f**, a compound selected on the basis of its greater

activity, shows a very favorable hydrogen bonding network (**Figure 8c**) that could be associated with a more effective interaction between the X—P(=Y)(ZR)$_2$ fragment (X = NH; Y = O, ZR = NH in **6f**) and the active site and surrounding cavity residues. In this derivative, as observed previously, the presence of the NO_2 substituent in the ortho aryl position can contribute greatly through its ability to stabilize the most favorable conformation for the interaction with the active site as a result of the bond formed with fragment X—P(=Y)(ZR)$_2$ as well as by the establishment of hydrogen bonds with the surrounding residues. The same interaction pattern is obtained for compound **6k**. In this compound, the heteroatoms in the benzothiazole ring contribute to the formation of the favorable network of hydrogen bonds.

The docking study carried out for the most voluminous compounds, the benzyloxy derivatives, is schematically summarized in **Figure 9**. In these cases the same superposition pattern as mentioned above was followed in the superposition of fragment X—P(=Y)(ZR)$_2$ for all of the representative low-energy conformations obtained in the conformational analysis. In the case of compound **1d** (X = O, Y = O, Z = NH_2) a greater number of conformations were detected with the appropriate orientation of the voluminous aryl unit toward the open cavity of the active center, and the lowest energy conformation is among these (**Figure 9a**). In contrast, for **6g** (X = NH, Y = O, Z = NH_2) a lower number of conformations with the favorable orientation is obtained and the lowest energy one is not among them. This could be related to the lower activity shown by **6g** (IC_{50} = 3.5 μM) in comparison to **1d** (IC_{50} = 0.016 μM).

On the basis of the studies carried out, the most effective urease inhibitors are the phosphoricamide derivatives that incorporate a flat aromatic ring, provided in ortho position with a group able to establish intramolecular hydrogen bridges with the free NH_2 terminal groups, and, in addition, with the surrounding residues in the active enzyme site. The ring must be united to the phosphoricamide moiety by a group, preferably NH, that makes it possible to adopt an appropriate conformation for an effective interaction with the active site and also to participate in the favorable hydrogen bond network.

In fact, the structural proposed requirements represent improvements in the activity of reference compounds NBPT and PPD. The data obtained in this study allowed us to corroborate the applicability of our starting hypothesis and the validity of the proposed structural model. These data will be used for the design of new compounds with greater effectiveness in the target biological activity.

LITERATURE CITED

(1) Witte, C. P.; Tiller, S. A.; Taylor, M. A.; Davies, H. V. Leaf urea metabolism in potato: urease activity profile and patterns of recovery and distribution of N-15 after foliar urea application in wild-type and urease-antisense transgenics. *Plant Physiol.* **2002**, *128*, 1129–1136.

(2) Ciurli, S.; Benini, S.; Rypniewski, W. R.; Wilson, K. S.; Miletti, S.; Mangani, S. Structural properties of the nickel ions in urease: novel insights into the catalytic and inhibition mechanisms. *Coord. Chem. Rev.* **1999**, *90—192*, 331–355.

(3) Estiu, G.; Merz, K. M. The hydrolysis of urea and the proficiency of urease. *J. Am. Chem. Soc.* **2004**, *126*, 6932–6944.

(4) Blakeley, R. L.; Zerner, B. Jack bean urease: the first nickel enzyme. *J. Mol. Catal.* **1984**, *23*, 263–292.

(5) Jabri, E.; Carr, M. B.; Hausinger, R. P.; Karplus, P. A. The crystal structure of urease from *Klebsiella aerogenes*. *Science* **1995**, *268*, 998.

(6) Benini, S.; Rypniewski, W. R.; Wilson, K. S.; Miletti, S.; Ciurli, S.; Mangani, S. A new proposal for urease mechanism based on the crystal structures of the native and inhibited enzyme from *Bacillus pasteurii*: why urea hydrolysis costs two nickels. *Struct. Fold. Des.* **1999**, *7*, 205–216.

(7) Benini, S.; Ciurli, S.; Nolting, H. F.; Mangani, S. X-ray absorption spectroscopy study of native and phenylphosphorodiamidate-inhibited *Bacillus pasteurii* urease. *Eur. J. Biochem.* **1996**, *239*, 61–66.

(8) Krajewska, B.; Zaborska, W. Jack bean urease: the effect of active-site binding inhibitors on the reactivity of enzyme thiol groups. *Bioorg. Chem.* **2007**, *35*, 355–365.

(9) Follmer, C. Insights into the role and structure of plant ureases. *Phytochemistry* **2008**, *69*, 18–28.

(10) Takishima, K.; Suga, T.; Mamiya, G. The structure of jack bean urease. The complete amino acid sequence, limited proteolysis and reactive cysteine residues. *Eur. J. Biochem.* **1988**, *175*, 151–165.

(11) Mobley, H. L. T.; Hausinger, R. P. Microbial ureases: significance, regulation, and molecular characterization. *Microbiol. Mol. Biol. Rev.* **1989**, *53*, 85–108.

(12) Antisari, L. V.; Marzadoni, C.; Gioacchini, P.; Ricci, S.; Gessa, C. Effect of the urease inhibitor *N-n*-butylthiophosphorictriamide on ammonia volatilization and evolution of mineral nitrogen. *Biol. Fert. Soils* **1996**, *22*, 196–201.

(13) Hendrickson, L. L.; Douglass, E. A. Metabolism of the urease inhibitor *N*-(*n*-butyl)thiophosphorictriamide (NBPT) in soils. *Soil Biol. Biochem.* **1993**, *25*, 1613–1616.

(14) Creason, G. L.; Schmitt, M. R.; Douglass, E. A.; Hendrickson, L. L. Urease inhibitory activity associated with *N*-(*n*-butyl)thiophosphoric triamide is due to formation of its oxon analog. *Soil Biol. Biochem.* **1990**, *22*, 209–211.

(15) Kot, M.; Zaborska, W.; Orlinska, K. Inhibition of jack bean urease by *N*-(*n*-butyl)thiophosphorictriamide and *N*-(*n*-butyl)phosphorictriamide: determination of the inhibition mechanism. *J. Enzyme Inhib.* **2001**, *16*, 507–516.

(16) Hendrickson, L. L.; Omholt, T. E.; O'Connor, M. J. Effect of phenylphosphorodiamidate on immobilization and ammonia volatilization. *Soil Sci. Soc. Am. J.* **1987**, *51*, 1067–1071.

(17) Manunza, B.; Deiana, S.; Pintore, M.; Gessa, C. The binding mechanism of urea, hydroxamic acid and *N*-(*n-butyl*)-phosphoric triamide to the urease active site. A comparative molecular dynamics study. *Soil Biol. Biochem.* **1999**, *31*, 789–796.

(18) Benini, S.; Rypniewski, W. R.; Wilson, K. S.; Ciurli, S.; Mangani, S. Structure-based rationalization of urease inhibition by phosphate: novel insights into the enzyme mechanism. *J. Biol. Inor. Chem.* **2001**, *6*, 778–790.

(19) Musiani, F.; Arnofi, E.; Casadio, R.; Ciurli, S. Structure-based computational study of the catalytic and inhibition mechanisms of urease. *J. Biol. Inorg. Chem.* **2001**, *3*, 300–314.

(20) Dominguez, M. J.; Sanmartin, C.; Font, M.; Palop, J.; San Francisco, S.; Urrutia, O.; Houdusse, F.; García-Mina, J. M. Design, synthesis and biological evaluation of phosphoramide derivatives as urease inhibitors. *J. Agric. Food Chem.* **2008**, *56*, 3721–3731.

(21) Accelrys Software Inc. *InsightII 2000*; San Diego, CA, 2000.

(22) Accerlys Software Inc. *Discovery Studio Modeling Environment*, release 1.7; San Diego, Ca, 2007.

(23) Hypercube, Inc. *Hyperchem Professional*; Gainesville, FL.

(24) Allen, F. H. CSD The Cambridge Structural Database: a quarter of a million crystal structures and rising. *Acta Crystallogr.* **2002**, *B58*, 380–388.

(25) Berman, H. M.; Westbrook, J.; Feng, Z.; Gilliland, G.; Bhat, T. N.; Weissig, H.; Shindyalov, I. N.; Bourne, P. E. The Protein Data Bank. *Nucleic Acids Res.* **2000**, *28*, 235–242.

(26) Bruno, I. J.; Cole, J. C.; Edgington, P.; Kessler, R. M.; Macrae, C. F.; McCabe, P.; Pearson, J.; Taylor, R. ConQuest: new software for searching the Cambridge Structural Database and visualizing crystal structures. *Acta Crystallogr.* **2002**, *B58*, 389–397.

(27) Macrae, C. F.; Edgington, P. R.; McCabe, P.; Pidcock, E.; Shields, G. P.; Taylor, R.; Towler, M.; Van de Streek, J. Mercury:

visualization and analysis of crystal structures. *J. Appl. Crystallogr.* **2006**, *39*, 453–457.
(28) Shi, S.; Yan, L.; Yang, Y.; Fisher-Shaulsky, J.; Thacher, T. An extensible and systematic force field, ESFF, for molecular modeling of organic, inorganic and organometallic systems. *J. Comput. Chem.* **2003**, *24*, 1059–1076.
(29) Dewar, M. J. S.; Zoebisch, E. G.; Healy, E. F.; Stewart, J. J. P. Development and use of quantum mechanical molecular models. 76. AM1: a new general purpose quantum mechanical molecular model. *J. Am. Chem. Soc.* **1985**, *107*, 3902–3909.
(30) Stewart, J. J. P. Optimization of parameters for semi-empirical methods I—method. *J. Comput. Chem.* **1989**, *10*, 209–220.
(31) Rocchia, W.; Sridharan, S.; Nicholls, A.; Alexov, E.; Chiabrera, A.; Honig, B. Rapid grid-based construction of the molecular surface for both molecules and geometric objects: applications to the finite difference Poisson−Boltzmann method. *J. Comput. Chem.* **2002**, *23*, 128–137.
(32) Gilson, M. K.; Honig, B. Calculation of the total electrostatic energy of a macromolecular system; solvation energies, binding energies, and conformational analysis. *Protein Struct. Funct. Genet.* **1988**, *4*, 7–18.
(33) Rocchia, W.; Alexov, E.; Honig, B. Extending the applicability of the nonlinear Poisson−Boltzmann equation: multiple dielectric constants and multivalent ions. *J. Phys. Chem. B* **2001**, *105*, 6507–6514.
(34) Mayo, S. L.; Olafson, B. D.; Goddard, W. A. Dreiding: a generic force field for molecular simulations. *J. Phys. Chem.* **1990**, *94*, 8897–8909.
(35) Brooks, B. R.; Bruccoleri, R. E.; Olafson, B. D.; States, D. J.; Swaminathan, S.; Karplus, M. CHARMM: A program for macromolecular energy, minimization, and dynamics calculations. *J. Comput. Chem.* **1983**, *4*, 187–217.
(36) MacKerell, A. D.; Brooks, B.; Brooks, C. L.; Nilsson, L.; Roux, B.; Won, Y.; Karplus, M. CHARMM: the energy function and its parameterization with an overview of the program. *The Encyclopedia of Computational Chemistry*; Schleyer, P. v. R., Eds.; Wiley: Chichester, U.K., 1998; Vol. 1, pp 271−277.
(37) Boschov, P.; Seidel, W.; Muradian, J.; Tominaga, M.; Paiva, A. C. M.; Juliano, L. Ionization constants and thermodynamic parameters of histidine and derivatives. *Bioorg. Chem.* **1983**, *12*, 34–44.
(38) Costa, J. M.; Lluch, J. M. The use of quantum mechanics calculations for the study of corrosion inhibitors. *Corros. Sci.* **1984**, *24*, 929–930.

Received for review June 10, 2008. Revised manuscript received July 30, 2008. Accepted July 30, 2008.

JF801786D